

NAVAL POSTGRADUATE SCHOOL Monterey, California



**Symmetrical Number System Phase
Sampled Interferometer
Direction Finding Antennas**

by

D. C. Jenn
P. E. Pace

February 20, 1998

Approved for public release; distribution is unlimited.

Prepared for: Center for Reconnaissance Research
Naval Postgraduate School
Monterey, California 93943

19980508 055

DTIC QUALITY INSPECTED

**NAVAL POSTGRADUATE SCHOOL
Monterey, California**

RADM Robert C. Chaplin
Superintendent

R. Elster
Provost

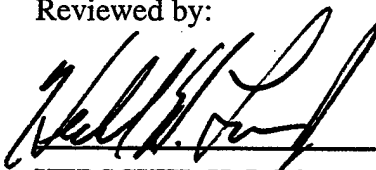
This report was sponsored by NPS Center for Reconnaissance Research.
Approved for public release; distribution is unlimited.

The report was prepared by:

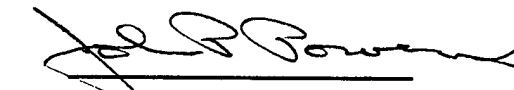

D. C. Jenn
Associate Professor
Department of Electrical and
Computer Engineering


P. E. Pace
Associate Professor
Department of Electrical and
Computer Engineering

Reviewed by:


HERSCHEL H. LOOMIS, JR.
Chairman
Department of Electrical and
Computer Engineering

Released by:


DAVID W. NETZER
Associate Provost and
Dean of Research

REPORT DOCUMENTATION PAGEForm Approved
OMB No. 0704-0188

Public reporting burden for the collection of information is estimated to average 1 hour per response, including the time for reviewing instructions, searching existing data sources, gathering and maintaining the data needed, and completing and reviewing the collection of information. Send comments regarding this burden estimate or any other aspect of this collection of information, including suggestions for reducing this burden to Washington Headquarters Services, Directorate for Information Operations and Reports, 1215 Jefferson Davis Highway, Suite 1204, Arlington VA 22202-4302, and to the Office of Management and Budget, Paperwork Reduction Project (0704-0188), Washington DC 20503.

1. AGENCY USE ONLY (Leave blank)	2. REPORT DATE February 20, 1998	3. REPORT TYPE AND DATES COVERED Technical Report	
4. TITLE AND SUBTITLE Symmetrical Number System Phase Sampled Interferometer Direction Finding Antennas		5. FUNDING NUMBERS N00173-98-WR-00140	
6. AUTHOR(S) D. C. Jenn and P. E. Pace			
7. PERFORMING ORGANIZATION NAME(S) AND ADDRESS(ES) Department of Electrical and Computer Engineering Naval Postgraduate School Monterey, CA 93943-5000		8. PERFORMING ORGANIZATION REPORT NUMBER NPS-EC-98-003	
9. SPONSORING/MONITORING AGENCY NAME(S) AND ADDRESS(ES) Center for Reconnaissance Research Department of Electrical and Computer Engineering Naval Postgraduate School Monterey, CA 93943		10. SPONSORING/MONITORING AGENCY REPORT NUMBER	
11. SUPPLEMENTARY NOTES The views expressed in this report are those of the author and do not reflect the official policy or position of the Department of Defense or the United States Government.			
12a. DISTRIBUTION/AVAILABILITY STATEMENT Approved for public release; distribution is unlimited.		12b. DISTRIBUTION CODE A	
13. ABSTRACT (Maximum 200 words) A novel phase-sampled interferometer direction finding (DF) antenna architecture is described. Based on the optimum symmetrical number system (OSNS) the analog spatial filtering operation is broken down into a number of parallel suboperations (moduli) that are of smaller complexity. One two-element interferometer is used for each suboperation and only requires a precision in accordance with its modulus. A much higher spatial resolution is achieved after the different OSNS moduli are used and the filtering results of these low precision suboperations are recombined. The use of the symmetrically folding phase waveform provides for a straight forward implementation of a high resolution DF antenna. Simulated and experimental results are shown to numerically evaluate the feasibility of the design. Spatial encoding errors that may occur due to the angle-of-arrival being located about a code transition point are also quantified.			
14. SUBJECT TERMS direction finding, interferometers, symmetrical number systems		15. NUMBER OF PAGES 28	16. PRICE CODE
17. SECURITY CLASSIFICATION OF REPORT UNCLASSIFIED	18. SECURITY CLASSIFICATION OF THIS PAGE UNCLASSIFIED	19. SECURITY CLASSIFICATION OF ABSTRACT UNCLASSIFIED	20. LIMITATION OF ABSTRACT SAR

1 Introduction

Direction finding (DF) systems provide an emitter's bearing that can be used as a sorting parameter in the identification of radar and communication systems. The emitter's true bearing gives an estimate of the geolocation (geographical direction) and can also be used in navigation and targeting [1]. Also, successful electronic attack depends on the ability of the associated electronic warfare support system to measure the direction to the victim emitter. Law enforcement and wildlife conservation efforts also employ DF systems, as do signal intelligence and search and rescue teams.

There are a number of tradeoffs in a DF antenna architecture. Among these are accuracy, response time, antenna size, and the associated cost. The accuracy depends largely on the signal characteristics and the errors generated by the system itself. Response time also depends on the architecture used and the bandwidth. Other important performance metrics are the processing gain and the probability of intercept. In a phase sampled system, the antenna performs the spatial sampling using either a linear or circular interferometer grid. The antenna size has also traditionally been a problem. For example, high frequency (HF) DF arrays typically require a large spacing between elements to obtain a fine spatial resolution. This large spacing between elements becomes a packaging problem due to platform restrictions.

The phase sampled linear interferometer is a well known DF approach [1-3] that consists of two perpendicular linear interferometers to obtain two angular coordinates. The DF algorithm uses different spacings within each array to obtain time-of-arrival relationships that translate into measurable phase differences that are used to determine the angle of arrival. Multiple baseline systems generally consist of a reference antenna in the center of two or more other antennas spaced at different distances. By

relating the baselines in a known manner the ambiguities may be resolved.

There is sufficient information from three elements to uniquely determine the angle of arrival (AOA). To resolve the ambiguities in phase sampling, a combination of phase and amplitude is most often required. Ambiguous measurements from a widely spaced pair are resolved by another more closely spaced baseline pair having no ambiguities. Fine angular measurements are possible with the pair having the larger spacing (greatest phase change per degree) while the unambiguous coarse angular measurements are made by the pair with the smaller spacing (smallest phase change per degree). The channel with the smallest phase change per degree often requires a better signal to noise ratio and an amplitude measuring system to provide the information [3]. The phase information often takes the form of a sawtooth folding waveform which is hard to detect with analog hardware. Analog mixers that provide the phase response in a symmetrical folding waveform are more convenient; however, there are more ambiguities that must be resolved.

This report describes the development of a new high-resolution phase-sampled DF array based on an *optimum symmetrical number system* (OSNS) [4]. Symmetrical number systems have been used previously to increase the efficiency of folding analog-to-digital converter architectures, efficiently encode digital antenna links, and increase the resolvable bandwidth of 2- and 3-channel digital intercept receivers [5-7]. The OSNS DF antenna architecture being investigated uses the OSNS to decompose the analog spatial filtering operation into a number of parallel sub-operations (moduli) that are of smaller complexity. One two-element interferometer is used for each sub-operation and only requires a precision in accordance with its modulus. A much higher spatial resolution is achieved after the spatial filtering results of the low precision sub-operations of all the OSNS moduli are recombined. The use of the symmetrically

folding phase waveform provides for a simple straight-forward implementation. In Section 2 we review the fundamentals of phase-sampled interferometers. The OSNS is then presented in Section 3. In Section 4 the design and operation of the OSNS DF antenna system is described. Simulation and experimental results are shown to numerically evaluate the transfer function of the antenna and detail the advantages of our approach.

2 Phase-Sampled Interferometers

A two-element linear interferometer is shown in Fig. 1. The two antenna elements are spaced a distance d apart and the plane wave arrives with incident angle ϕ_B . In this phase monopulse configuration the angle ϕ_B is measured from the perpendicular to the baseline axis and can take on values $\pi/2 < \phi_B < -\pi/2$. The electromagnetic wave arrives first at antenna element 1 located at $x = d/2$ and $y = 0$. Without affecting the general case we assume that the phase of the wave arriving at the first element at time t is $\psi_1 = 2\pi ft$. The wave arrives at antenna element 2 after traveling an additional distance of $d \sin \phi_B$. The phase of the wave arriving at the second element is then

$$\psi_2 = 2\pi ft - \frac{2\pi}{\lambda} d \sin(\phi_B). \quad (1)$$

The phase difference between the two elements is

$$\Delta\psi = \psi_1 - \psi_2 = 2\pi \frac{d}{\lambda} \sin(\phi_B) \quad (2)$$

which is a function of the incidence angle of the wave. For example, a plane wave arriving perpendicular to the array axis would result in a phase difference of zero.

The signals received by the antenna elements are mixed (multiplied together and processed by a lowpass filter) resulting in an output signal whose frequency is the

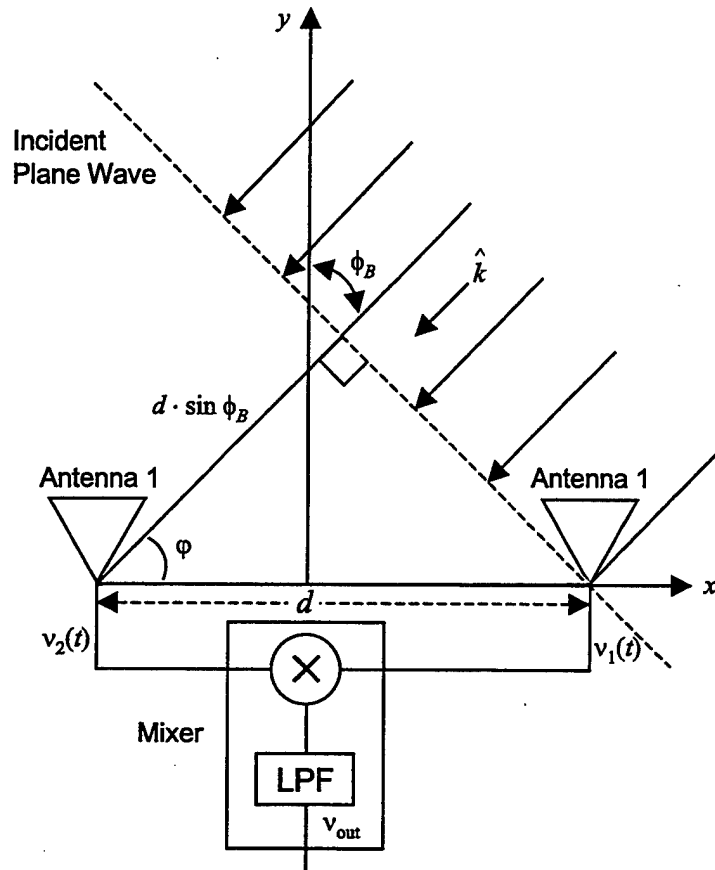


Figure 1: Linear two-element interferometer array geometry.

difference between the two input signal frequencies. Because the signals have the same frequency, the mixer output is a voltage whose value is proportional to the difference between signal phases ψ_1 and ψ_2 . This difference is not purely $\Delta\psi$ because of the time delays due to the different transmission line lengths from each antenna element. However, these line lengths are known and can be compensated for in the angle estimate.

Let the signals from the two antenna elements be

$$v_1(t) = V \cos [2\pi ft + \phi_1(t)] \quad (3)$$

and

$$v_2(t) = V \cos [2\pi ft + \phi_2(t)] \quad (4)$$

where V is the maximum value of the voltage at the antenna elements. Let ψ_0 be the phase difference between the transmission lines to the two elements. The lowpass mixer output voltage is

$$\begin{aligned} v_{\text{out}} &= \frac{V^2}{2} \cos(\Delta\phi) \\ &= \frac{V^2}{2} \cos\left(\frac{2\pi d}{\lambda} \sin(\phi_B) + \psi_0\right) \end{aligned} \quad (5)$$

which contains the plane wave AOA information. For values of $d = \lambda/2$ and $\psi_0 = 0$, $\Delta\phi = \pi \sin(\phi_B)$. As the AOA (ϕ_B) varies from $-\pi/2$ to $\pi/2$, the phase difference ($\Delta\phi$) varies from $-\pi$ to π as shown in Fig. 2. The mixer output voltage, which is a function of the phase difference, is a symmetrical folding waveform, as shown in Fig. 3. Together these relationships give the mixer output voltage as a function of the angle of arrival as shown in Fig. 4 for $d = \lambda/2$.

Ambiguities are generated for baselines where $d > \lambda/2$. For example, the output voltage for $d = 7.5\lambda$ is shown in Fig. 5. A given output voltage is highly ambiguous

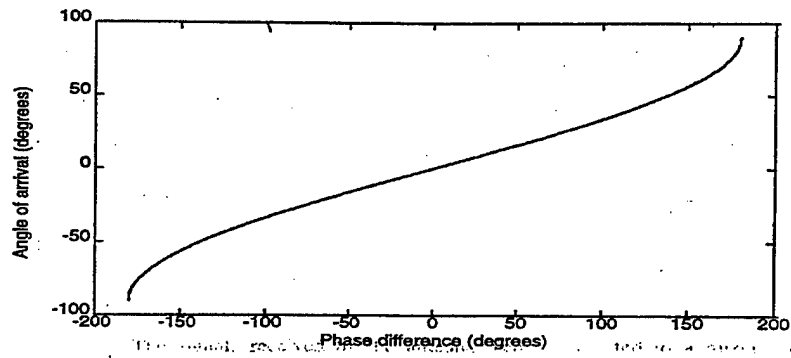


Figure 2: Angle of arrival vs. phase difference between the elements for $d = \lambda/2$.

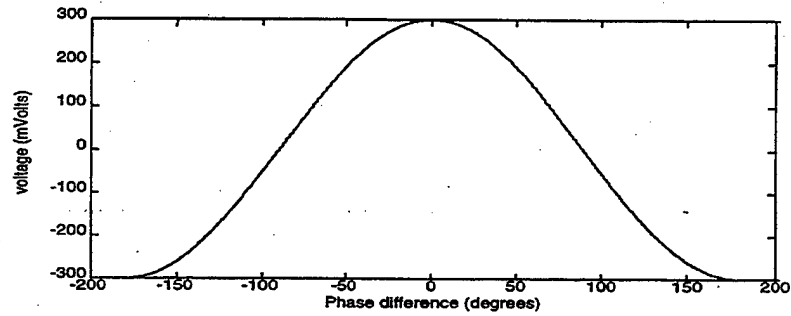


Figure 3: Phase difference between the elements vs. mixer output voltage for $d = \lambda/2$.

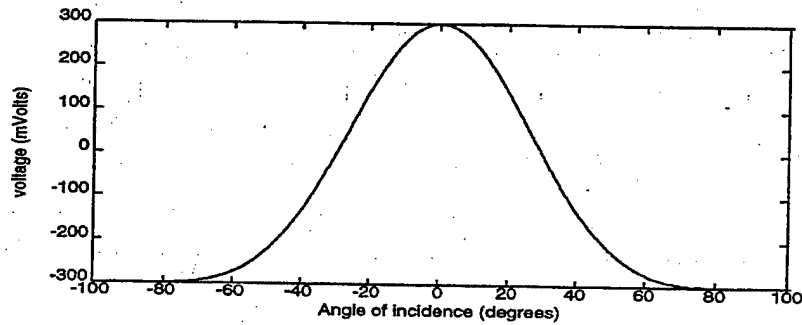


Figure 4: Angle of arrival vs. mixer output voltage for $d = \lambda/2$.

since it corresponds to many angles of arrival. The number of periods n that occur in 180° is

$$n = \frac{2d}{\lambda}. \quad (6)$$

For $d = 7.5\lambda$, $n = 15$ folds are available as shown in Fig. 5. The folding period is not constant but grows larger in proportion to the angle off of broadside (because of the $\sin \phi_B$ dependence in Eq. (5)).

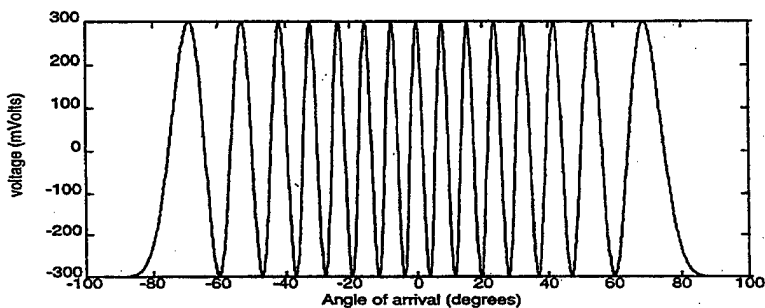


Figure 5: Angle of arrival vs. mixer output voltage for $d = 7.5\lambda$.

The ambiguities within the symmetrical folding waveforms represent the phase difference between the elements and can be resolved by using additional interferometers in the linear array. Each interferometer symmetrically folds the input signal phase to be sampled. Figure 6(a) shows a schematic diagram of a 4-bit system that uses four interferometers (one interferometer per bit). Detailed are the most significant bit (MSB), the next most significant bit (NMSB), the next least significant bit (NLSB), and the least significant bit (LSB). The plane wave for which the AOA is to be determined is applied in parallel to each interferometer. High-speed binary comparators are used to produce a digital Gray code output. Each interferometer in the linear array symmetrically folds the phase response with the folding period between interferometers being a successive factor of two. The folding waveforms are shifted

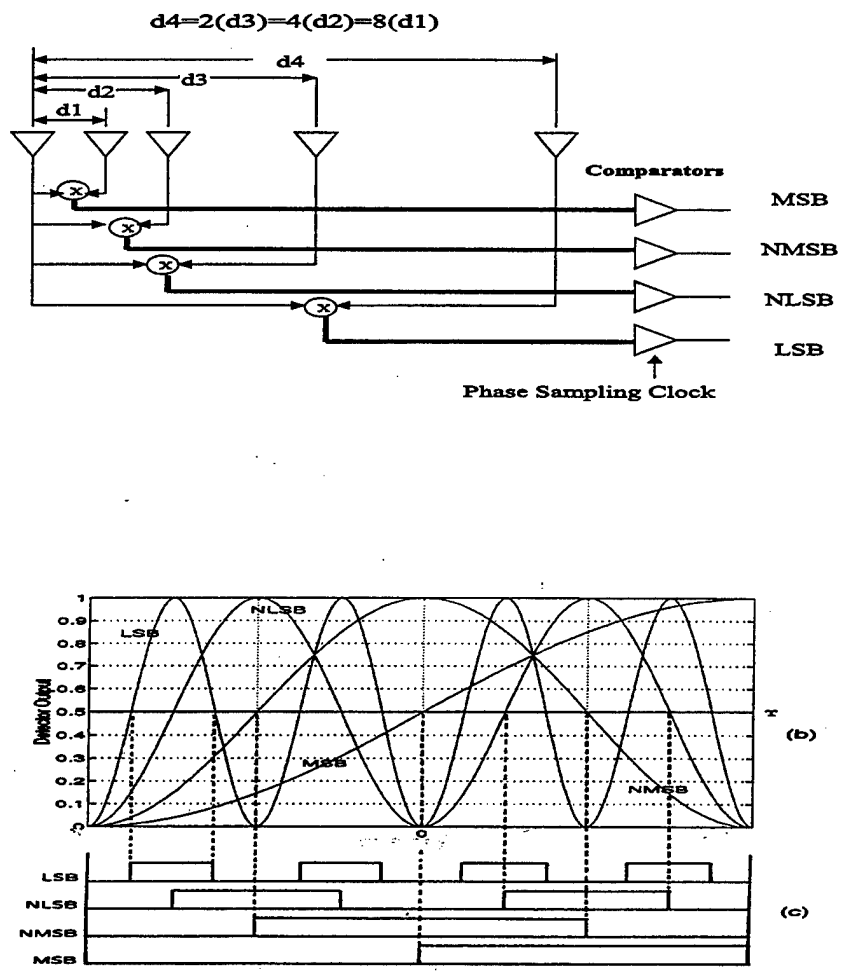


Figure 6: Binary Gray code phase sampled interferometer array: (a) Block diagram of 4-bit architecture, (b) simulated phase response from mixers and, (c) corresponding binary Gray code.

appropriately using a phase shifter in each channel to achieve the Gray code results. Figure 6(b) shows the symmetrically folded phase signals that appear at the output of each mixer. The folded output from each mixer (phase response) is then quantized with a single comparator with normalized threshold level $T = 0.5$. Together, the comparator outputs directly encode the signal's AOA in the Gray code format. Figure 6(c) shows the resulting comparator outputs. These architectures make use of the periodic dependence of the interferometer's phase response on the applied plane wave's AOA and the distance between the elements of each interferometer.

One of the major limitations associated with this type of approach is the achievable resolution. For the folding periods to be a successive factor of 2, the distance between the elements must also be doubled. That is, an 8-bit DF antenna using the previous scheme would require element spacings $\lambda/4, \lambda/2, \lambda, 2\lambda, 4\lambda, \dots, 32\lambda$ with a total baseline length of 32λ . This distance doubling requirement of the element spacings (complex analog hardware) adversely affects the physical implementation of the DF architecture and ultimately constrains the achievable resolution. Incorporation of the OSNS encoding process discussed next overcomes the major limitations of the binary encoding approach and provides an efficient method to enhance the resolution of the array.

3 Optimum Symmetrical Number System

The optimum SNS scheme is composed of a number of pairwise relatively prime (PRP) moduli m_i . The integers within each OSNS modulus are representative of a symmetrically folded waveform with the period of the waveform equal to *twice* the PRP modulus, i.e., $2m_i$. For given m , the integer values within twice the individual

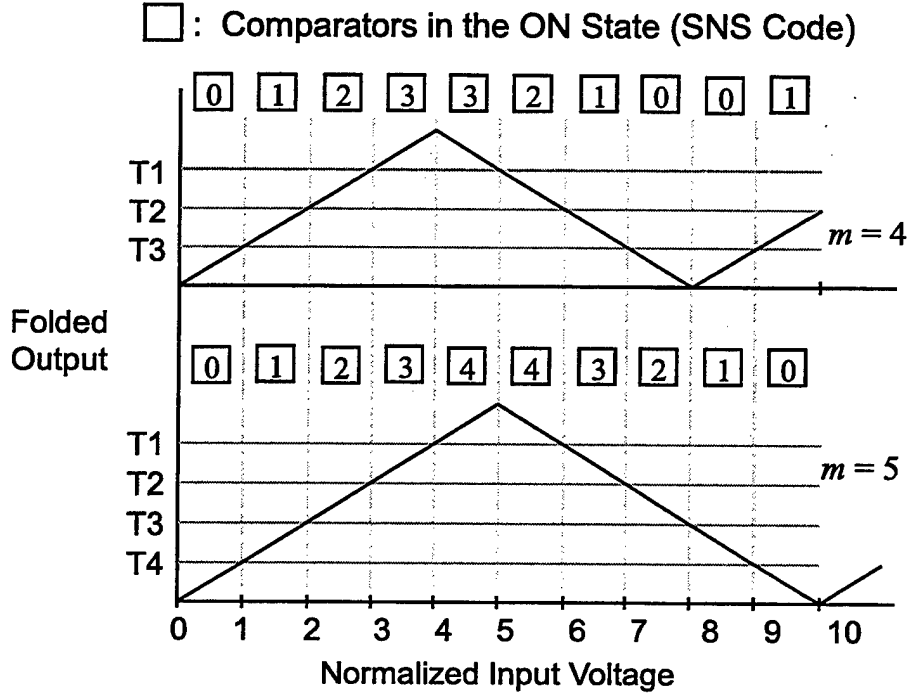


Figure 7: Optimum SNS folding waveforms and output codes for $m_1 = 4$ and $m_2 = 5$.

modulus are given by the row vector

$$\bar{x}_m = [0, 1, \dots, m-1, m-1, \dots, 1, 0]. \quad (7)$$

Figure 7 shows the OSNS folding waveforms and output codes for both $m_1 = 4$ and $m_2 = 5$. Due to the presence of ambiguities, the integers within (7) do not form a complete system of length $2m$ by themselves. The ambiguities that arise within the modulus are resolved by considering the paired values from all channels together. By recombining the N channels, the SNS is rendered a complete system having a one-to-one correspondence with the residue number system (RNS). For N equal to the number of PRP moduli, the dynamic range of this scheme is

$$M = \prod_{i=1}^N m_i. \quad (8)$$

Table 1: OSNS Dynamic Range with $m_1 = 4$ and $m_2 = 5$ ($M = 20$)

Normalized Input	$m_1 = 4$	$m_2 = 5$
0	0	0
1	1	1
2	2	2
3	3	3
4	3	4
5	2	4
6	1	3
7	0	2
8	0	1
9	1	0
10	2	0
11	3	1
12	3	2
13	2	3
14	1	4
15	0	4
16	0	3
17	1	2
18	2	1
19	3	0
20	3	0
21	2	1

 Ambiguity

This dynamic range is also the position of the first repetitive moduli vector. For the example with $m_1 = 4$ and $m_2 = 5$, the first repetitive moduli vector occurs at an input of 20 as indicated in Table 1. In the next section the OSNS is used to design a high resolution DF array requiring considerably less analog hardware than previous phase sampled DF designs.

4 OSNS Direction Finding Antenna Design

An N -channel OSNS phase-sampled DF antenna has $N + 1$ radiating elements, a microwave beamforming network, and a digital processor to recombine the phase samples

from the individual channels. Figure 8 shows a block diagram of an OSNS antenna that passively detects an emitter using N wideband interferometers (channels) that share a common element. As demonstrated below, very fine spatial resolution can be obtained by using two or three interferometers. The trade-off issues are discussed in the next section.

To provide an adequate amount of signal to noise, a low-noise amplifier is included at the output of each interferometer element. Since the common element splits the signal into N paths, an attenuator is placed in the other branches to balance the amplitudes. A fixed phase shifter is also included in one branch of each interferometer so that the symmetrically folded phase response waveforms from each mixer may be aligned. The alignment insures that the comparators in the digital processor properly sample the phase waveform and encode the angle-of-arrival in the OSNS. Also, since phase waveforms are bipolar, a dc bias amplifier is required at the output of the mixer to shift the folding waveforms to be above zero (unipolar). This is necessary since the comparator matching threshold values can not be near either the ground voltage or the supply voltage.

The OSNS encoding is affected by the distance between the interferometer elements and the small number of comparators that are used for each channel. The distance between the elements generates the required folding periods. If the desired number of spatial resolution cells (i.e., dynamic range of the OSNS) is M , then the required number of folds from each interferometer is

$$n_i = \frac{M}{2m_i} \quad (9)$$

where m_i is the corresponding channel modulus. The distance between the interfer-

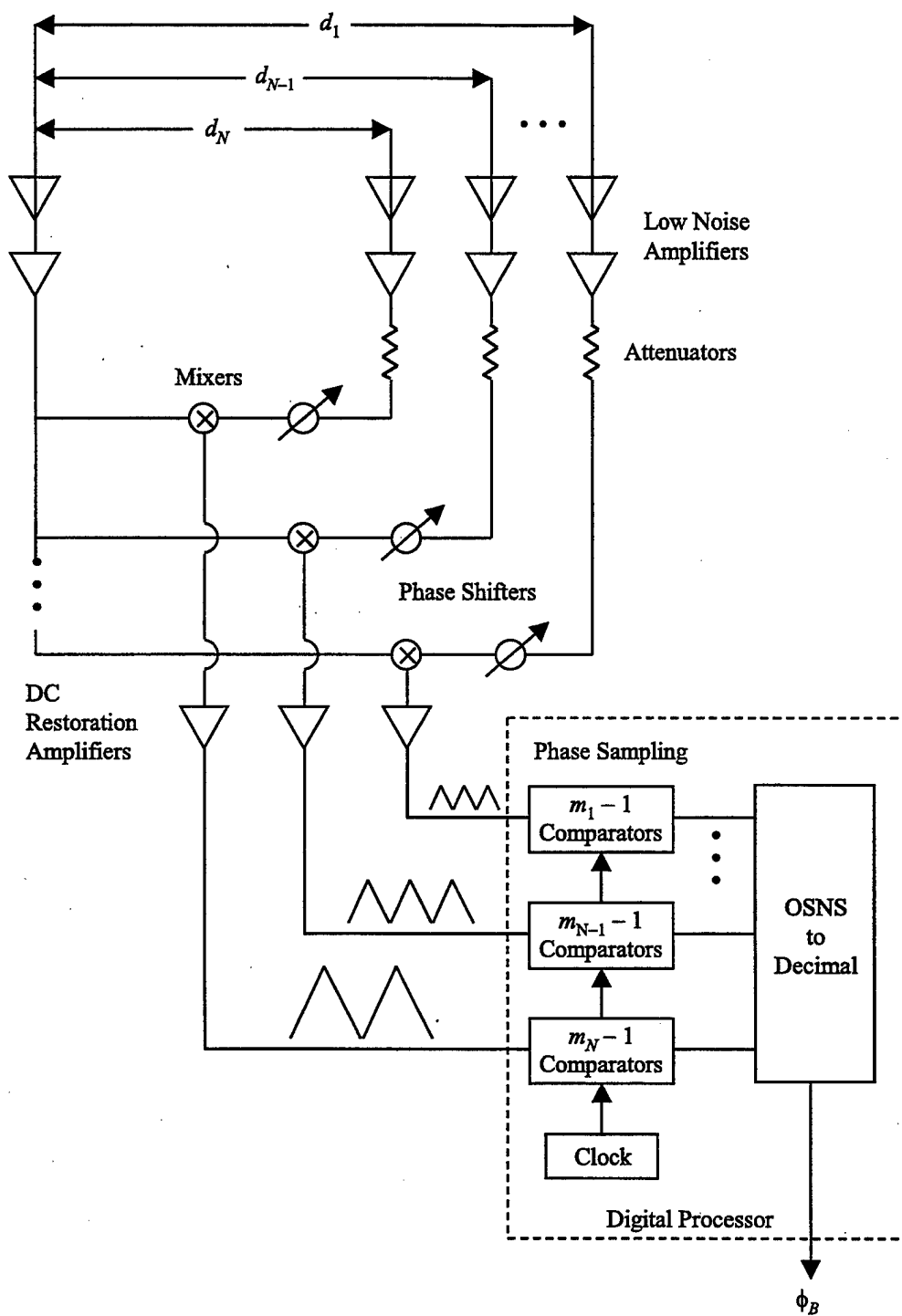


Figure 8: Optimum symmetrical number system, phase-sampled interferometer antenna architecture.

ometer elements becomes

$$d_i = \frac{n_i \lambda}{2} = \frac{M \lambda}{4m_i}. \quad (10)$$

The corresponding number of comparators required from (7) is $m_i - 1$. Note that for a given number of spatial resolution elements M , a larger modulus gives a smaller required distance between the interferometer elements. As an example, if a three moduli system is designed with $m_1 = 3$, $m_2 = 4$, and $m_3 = 5$, then the number of spatial resolution cells is 60. The total number of comparators required is 9. The spatial resolution near boresight is given by

$$r = \frac{\text{FOV}}{M} \quad (11)$$

where FOV is the field of view determined by the receiving element pattern. Ideally the FOV can be 180° , which gives $r = 3$ degrees.

5 Two-Channel Design

A $N = 2$ interferometer array was designed and fabricated. It has a shorter baseline than the example just described and because it has one less element it requires two less amplifiers (the amplifiers are a cost driver because they must be phase matched at all frequencies across the operating band). The two-channel high resolution OSNS DF array configuration is shown in Fig. 9. The short-baseline array uses relatively prime moduli $m_1 = 6$ and $m_2 = 11$ resulting in a total array length of 3.82 inches with spatial broadside resolution on the order of $r = 180/(6 \cdot 11) = 2.72$ degrees. For moduli $m_1 = 6$ and $m_2 = 11$, a total of $5 + 10 = 15$ comparators are now required (as compared to 9 comparators for the $n = 3$ example). This comparison illustrates the inherent flexibility in the OSNS for encoding wideband high-resolution DF arrays.

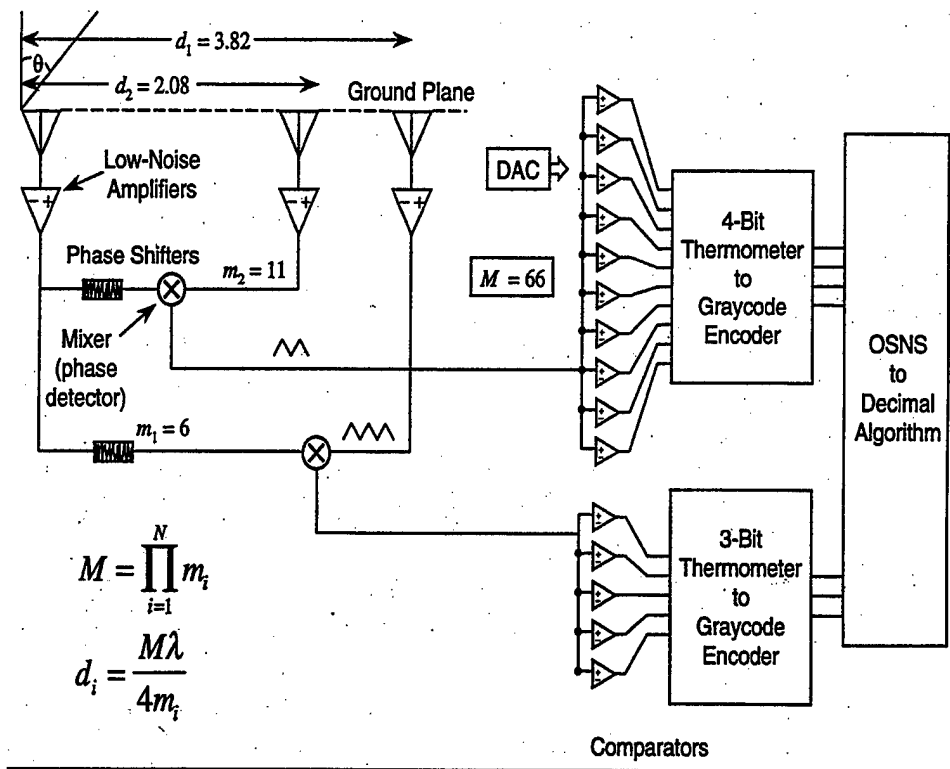


Figure 9: Schematic diagram of the $N = 2$ channel OSNS antenna array.

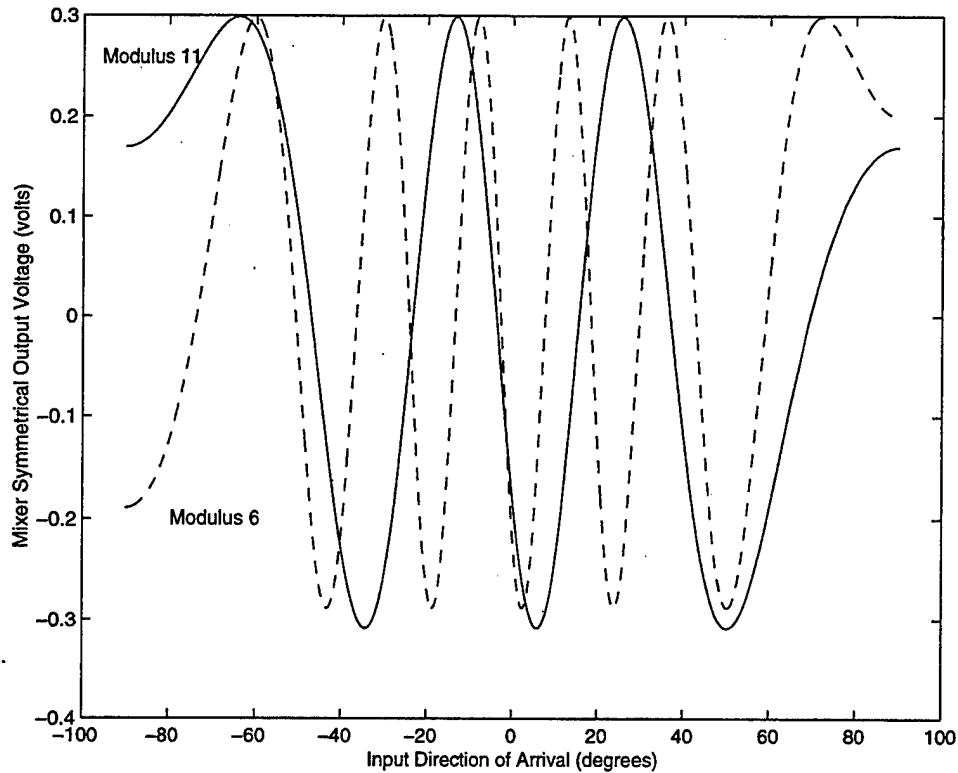


Figure 10: Simulated mixer output voltages for both $m_1 = 6$ and $m_2 = 11$.

To investigate the performance of the design, a simulation was carried out on the two-channel design. The folding waveforms representing the phase response in each channel are shown together in Fig.10. The sampling period is 0.1 degree for both curves. Note the edge effects that are present at the end-fire locations. Since these parts of the antenna response give erroneous results, the phase responses for both channels were aligned at an input direction of arrival of 50 degrees. This is also the point at which the OSNS encoding begins.

The comparator thresholds for each channel are non-uniformly spaced and are shown in Table 2. Using these threshold values and the simulated folding waveforms, the transfer function is computed and is shown in Fig. 11. Note the presence of the encoding errors when the sampled angle of arrival occurs about the code transition

Table 2: Comparator Thresholds for OSNS Antenna

$m_2 = 11$	$m_1 = 6$
$t_1 = -0.300122$	-0.258821
$t_2 = -0.277011$	-0.187919
$t_3 = -0.233625$	-0.012512
$t_4 = -0.165201$	0.143976
$t_5 = -0.04046$	0.26828
$t_6 = 0.050343$	
$t_7 = 0.149914$	
$t_8 = 0.212881$	
$t_9 = 0.264524$	
$t_{10} = 0.298688$	

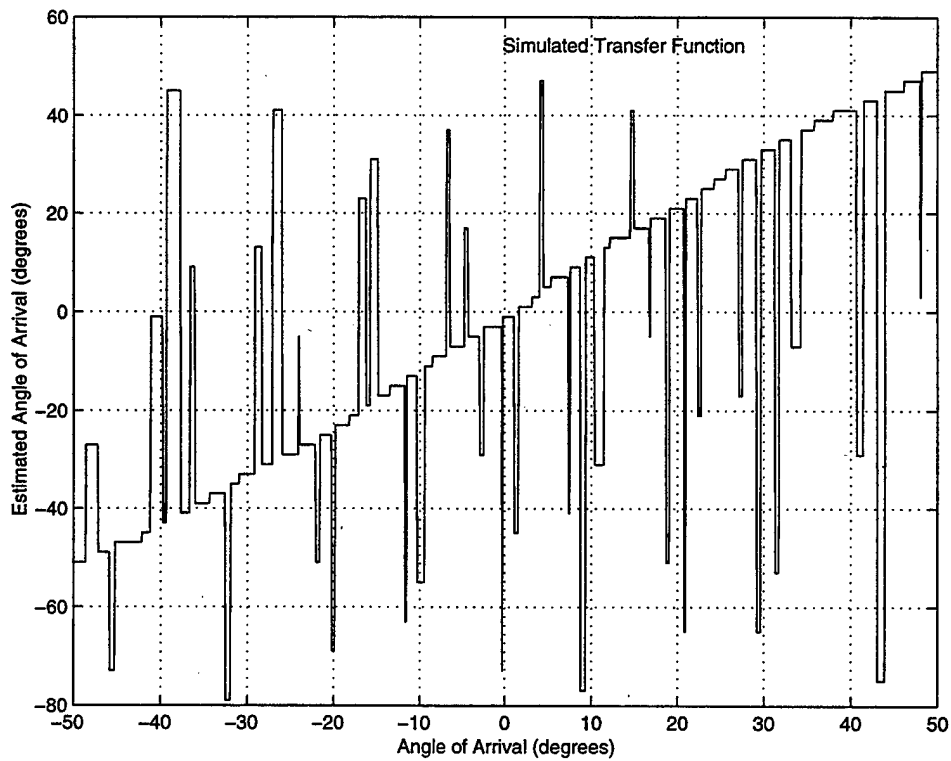


Figure 11: Simulated transfer function for OSNS antenna using $m_1 = 6$ and $m_2 = 11$.

points. These occur when some of the comparators that are supposed to change do not and thus cause a large error in the resolved AOA. Interpolation and other SNS encodings, however, can eliminate these occurrences.

6 Experimental Results

First, the amplifiers used in the $N = 2$ array design were characterized by examining the output power as a function of input power. The individual transfer functions of the six amplifiers being used are shown in Fig. 12. To insure that the response remains constant over a large range of input power, a (matched) pair of amplifiers are cascaded together with a 30 dB attenuator. This gives the desired flat response also shown in Fig. 12.

The $N = 2$ OSNS antenna was designed and built to operate at 8.5 GHz using open ended waveguide elements on an aluminum ground plane. Figure 13 shows the mixer output voltages for the two channels. Note the similarity to the simulated folding waveforms shown in Fig. 10. The major difference between the experimental results and simulated results is at wide angles. The corresponding transfer function of the array is shown in Fig. 14. The encoding errors in Fig. 11 are also present in the experimental result. They do, however, occur with different amplitudes and positions within the AOA due to the differences with phase response in each channel. It must be emphasized that the encoding errors are correctable.

7 Summary and Conclusions

A new direction finding architecture based on the optimum symmetrical number system has been presented. Equations (8) through (11) describe the tradeoff involved in the design of a OSNS array. The spatial resolution, that is, the angular resolution

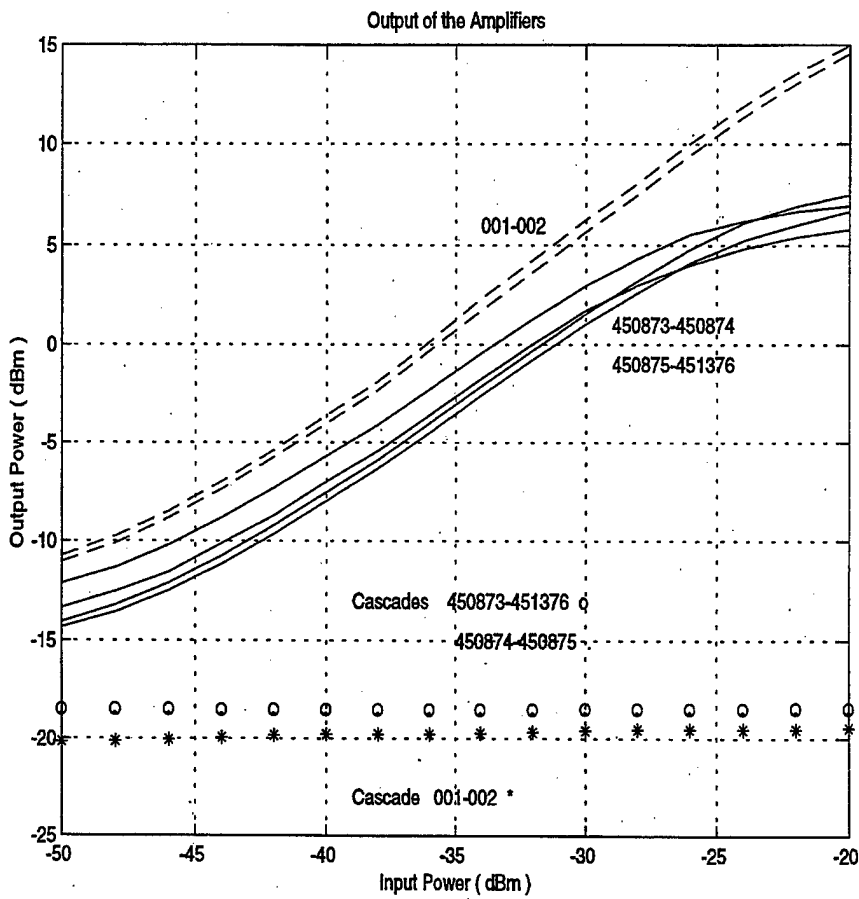


Figure 12: Transfer function of the six amplifiers being used in the OSNS antenna design.

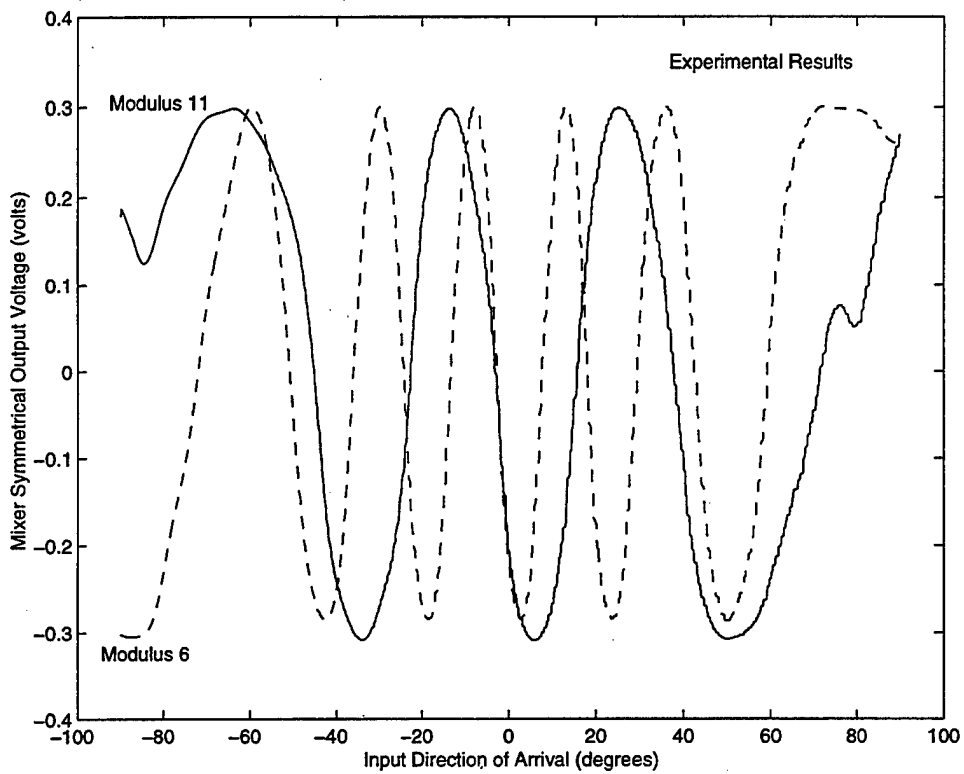


Figure 13: Experimental mixer output voltages.

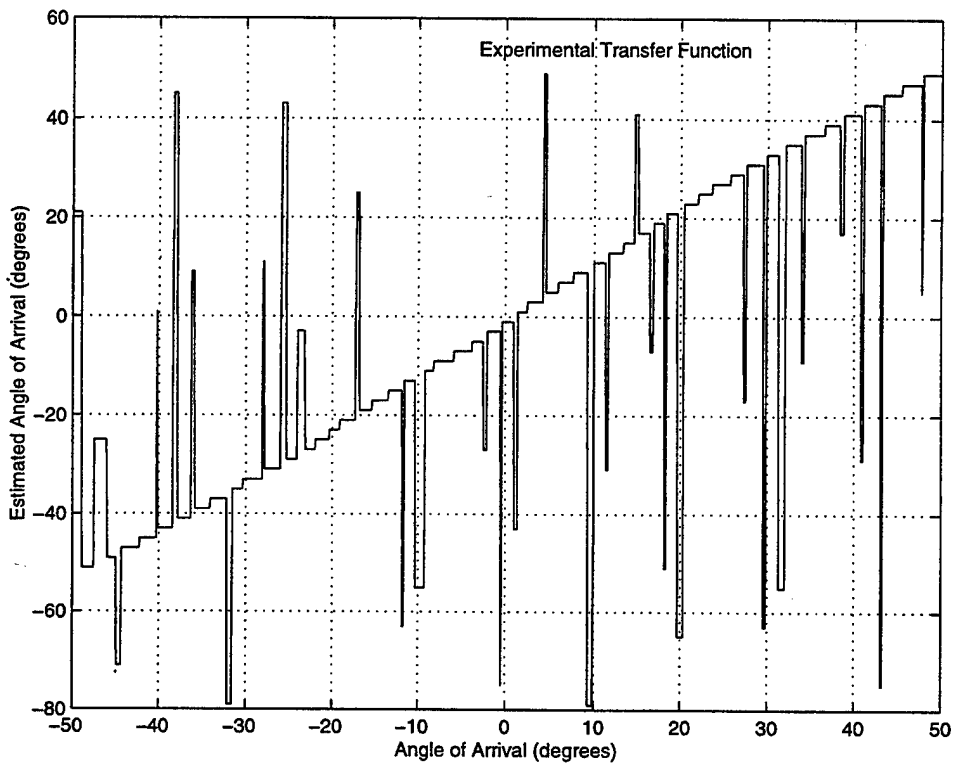


Figure 14: Experimental OSNS antenna transfer function.

of the direction measurement, is determined by M . The resolution is commonly expressed in bits, B . Thus the equivalent number of bits resolution is obtained from $M = 2^B$.

According to (8), M can be increased by

1. increasing the number of moduli, or
2. increasing the values of the individual moduli.

Since each m_i in (8) is equivalent to a channel, to increase M without adding antenna elements implies option 2.

The spacing of the elements is specified in (10). Generally, large m_i result in small spacings. The number of comparators required for the channel with modulus m_i is $m_i - 1$. Thus the total number of comparators is $\sum_{i=1}^N (m_i - 1)$. In general, as m_i decreases, the channel spacing decreases but the number of comparators increases.

The basic tradeoffs are illustrated in Fig. 15 for two and three channel arrays. The solid line is classical Rayleigh resolution limit, λ/d_{\max} , where d_{\max} is the distance between the farthest elements in the array. Each circle represents an OSNS array design based on a set of two (for $N = 2$) or three (for $N = 3$) relatively prime integers less than 50. The appeal the OSNS architecture is its flexibility and ability to provide high resolution with as few as three closely spaced elements. Even finer spatial resolution can be obtained for shorter baselines when integers greater than 50 are included. In practice, the element spacings will be limited by the size of the antenna elements themselves.

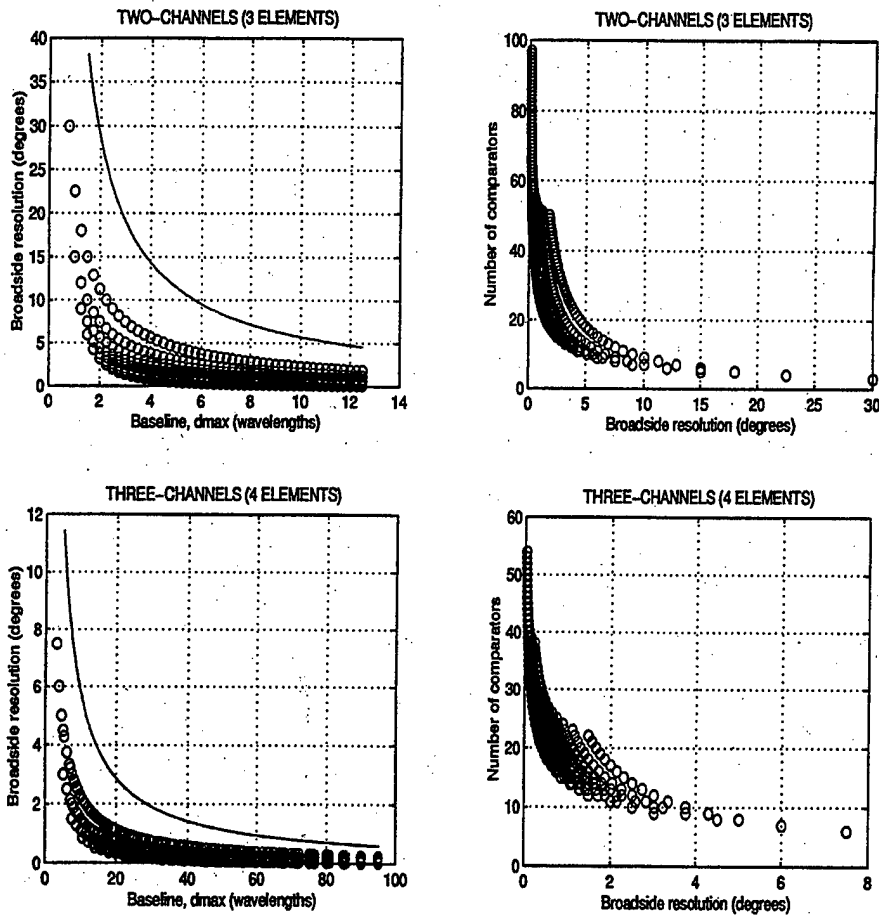


Figure 15: Basic trade-offs for two ($N = 2$) and three ($N = 3$) channel arrays for combinations of relatively prime integers less than 50. Each circle represents a unique OSNS configuration.

References

- [1] S. Lipsky, *Microwave Passive Direction Finding*, Chap. 6, Wiley, 1987.
- [2] R. Johnson and G. Miner, "Algorithms for Radio Direction Finding," *IEEE Trans. on Aero. and Elect. Sys.*, Vol. AES-22, No. 4, p. 432, July 1986.
- [3] E. Jacobs and E. Ralston, "Ambiguity Resolution in Interferometry," *IEEE Trans. on Aero. and Elect. Sys.*, Vol. AES-17, No. 6, p. 766, Nov. 1981.
- [4] P. Pace, J. Schafer, and D. Styer, "Optimum Analog Preprocessing for Folding ADCs," *IEEE Trans. on Circuits and Systems - II: Analog and Digital Signal Processing*, Vol. 42, pp. 825-829, Dec. 1995.
- [5] P. Pace, P. Ramamoorthy, and D. Styer, "A Preprocessing Architecture for Resolution Enhancement in High-Speed Analog-to-Digital Converters," *IEEE Trans. on Circuits and Systems - II: Analog and Digital Signal Processing*, Vol. 41, pp. 373-379, June 1994.
- [6] P. Pace, W. Ringer, K. Foster, and J. Powers, "Optical Signal Integrity and Interpolation Signal Processing in Wideband SNS Digital Antennas," *Proc. 1997 DARPA Photonic Systems for Antenna Applications*, Jan. 13, 1997.
- [7] P. Pace, R. Leino, and D. Styer, "Use of the Symmetrical Number System in Resolving Single-Frequency Undersampling Aliases," *IEEE Trans. on Signal Processing*, Vol. 45, pp. 1153-1160, May 1997.

INITIAL DISTRIBUTION LIST

	No. Copies
1. Defense Technical Information Center 8725 John J. Kingman Rd, STE 0944 Ft. Belvoir, VA 22060-6218	2
2. Dudley Knox Library, Code 52 Naval Postgraduate School 411 Dyer Road Monterey, CA 93943-5101	2
3. Research Office, Code 09 Naval Postgraduate School 589 Dyer Road Monterey, CA 93943-5138	1
4. Chairman, Code EC Department of Electrical and Computer Engineering Naval Postgraduate School 833 Dyer Road Monterey, CA 93943-5121	1
5. Director, Center for Reconnaissance Research Department of Electrical and Computer Engineering Naval Postgraduate School 833 Dyer Road Monterey, CA 93943-5121	7
6. Professor D. C. Jenn, Code EC/Jn Department of Electrical and Computer Engineering Naval Postgraduate School 833 Dyer Road Monterey, CA 93943-5121	2
7. Professor P. E. Pace, EC/Pc Department of Electrical and Computer Engineering Naval Postgraduate School 833 Dyer Road Monterey, CA 93943-5121	2